Electrical Demonstration of Sn-S-Based OTS Materials from Theoretical Design for Sustainable Innovation

Daniele Garbin, Taras Ravsher, Wouter Devulder, Sergiu Clima, Goedele Potoms, Attilio Belmonte, Gouri S. Kar

***Abstract*— In this work, we experimentally validate our theoretical framework for the ab-initio screening of new, sustainable materials for Ovonic Threshold Switch (OTS) applications, avoiding elements such as As and Se that are associated with a high health and safety risk. We demonstrate that the newly designed Sn-S-based OTS ternary alloys are electrically functional, and investigate the links between material properties and electrical performance. Results indicate that the Sn-S material system is a promising candidate for OTS selector and memory applications. Our findings open new research paths for further composition optimization aimed at bridging the performance gap with state-of-the-art materials based on As and Se. The experimental results will enable further refinement of the theoretical model and improve its prediction capabilities.**

***Index Terms*—Threshold switching, Ovonic threshold switching, OTS, selector.**

I. Introduction

IN recent years, the semiconductor industry has been actively exploring sustainable alternative materials by limiting the use of toxic elements in various electronic applications. As part of this ongoing effort, our research group conducted a systematic and comprehensive investigation to identify novel ovonic threshold switching (OTS) ternary materials, specifically excluding toxic elements such as As and Se.

In our previous publications [1, 2], we introduced an ab-initio screening methodology that allowed us to efficiently narrow down the extensive pool of potential chemical compositions to a short-list of most promising candidates. By utilizing physics-based material parameters related to OTS behavior, including material stability, electronic properties, and changes in polarizability, we introduced the concept of the OTS gauge. This condensed matter physics parameter served as a valuable tool to estimate the likelihood of a material exhibiting OTS behavior. The ab-initio screening methodology consists of a cascade of 8 filters as illustrated in Figure 1: undesirable/ toxic element exclusion, OTS-compatible electronic configuration (5 valence electron rule), phase stability of the amorphous alloys at BEOL temperatures (high glass-transition temperature), high chemical stability (negative formation enthalpy), low leakage current (open trap gap), immunity to phase demixing (low spinodal temperature), application-compatible trap/mobility gaps, and OTS behavior indicator (OTS gauge) [1,2].

As a result of our comprehensive investigation, we identified a set of 12 highly promising ternary compositions that are free from As and Se. These compositions showed good potential as OTS selector materials for Resistive Random Access Memory (RRAM) applications. Building upon these findings, our present study focuses on the experimental demonstration of the functionality of devices based on some of the materials identified in our previous publications. Specifically, since out of the 12 down-selected compositions, 4 are Sn-S-based, we target this material family and its alloys with N, Ge, and Si.

We decided to focus on a limited set of compositions out of the 12 candidate materials for experimental study due to resource constraints, specifically the number of PVD sputtering targets that can be used at the same time. Our current PVD deposition setup allows for the co-sputtering of only a finite number of compositions simultaneously. Given these hardware limitations, we prioritized co-sputtering from Si, Ge, and SnS2 targets, while another sputtering target in the same deposition chamber is dedicated to the in-situ deposition of the carbon-based top electrode. This setup constrained our ability to explore a broader range of materials in the current study. However, future work will aim to extend the set of materials studied experimentally, leveraging additional resources and potentially different deposition techniques to cover a wider selection of promising compositions identified in our theoretical screening.

In this paper, we aim to bridge the gap between theoretical predictions and practical implementation by presenting experimental evidence supporting the suitability of these As/Se-

This paragraph of the first footnote will contain the date on which you submitted your paper for review. It will also contain support information, including sponsor and financial support acknowledgment.”

D. Garbin, W. Devulder, S. Clima, G. Potoms, A. Belmonte, and G. S. Kar are with imec, Kapeldreef 75, 3001 Leuven, Belgium (e-mail: daniele.garbin@imec.be).

T. Ravsher is with imec, 3001 Leuven, Belgium, and with the Department of Physics and Astronomy, KU Leuven, 3001 Leuven, Belgium

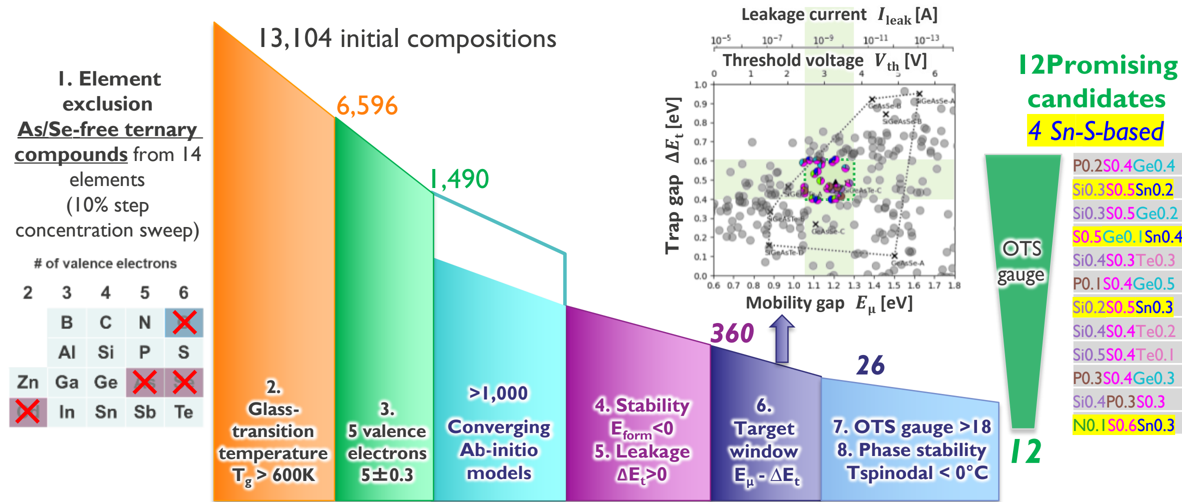

Fig.1. Summary of our ab-initio OTS material screening methodology [1,2], consisting of 8 cascaded selection filters, resulting in a set of 12 promising compositions. 4 out of 12 are Sn-S based and investigated experimentally in this paper. Inset: highlight of the targeted trap/mobility gap window.

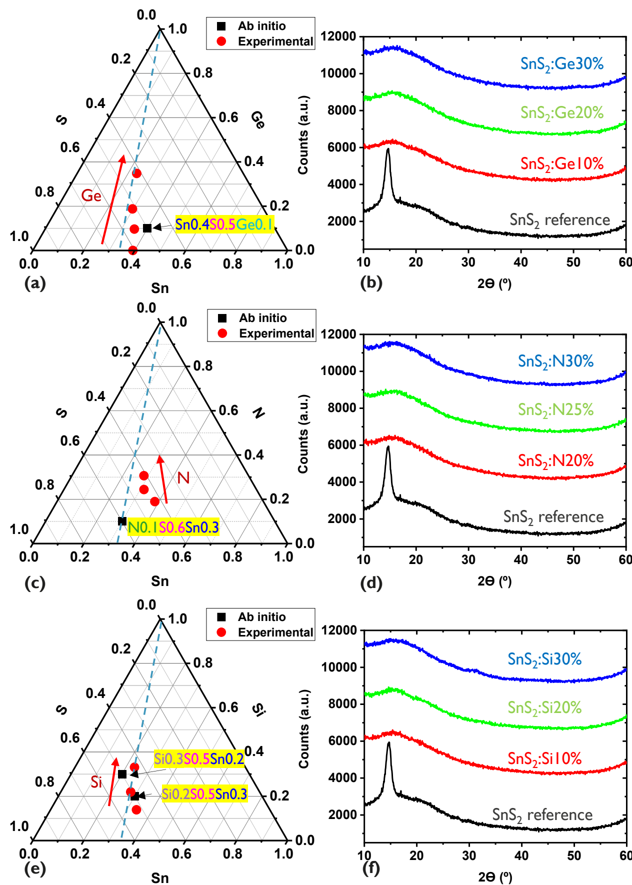

Fig.2. Ternary diagrams for (a) Sn-S-Ge, (b) Sn-S-N, (c) Sn-S-Si material systems. The dashed line indicates the SnS_2 tie line. Square symbols indicate the ab initio compositions, circles indicate the experimental compositions. XRD spectra for (b) Sn-S-Ge, (d) Sn-S-N, (f) Sn-S-Si. While the SnS_2 reference film is crystalline, the absence of peaks in the XRD spectra for the newly developed materials indicates that the films are amorphous as intended.

TABLE I
COMPOSITION DETAILS OF THE DEPOSITED FILMS

(a) Sn-S-Ge compositions from RBS:

Label	Sn	S	Ge
SnS_2	39.3%	60.7%	0.0%
SnS_2:Ge10%	35.0%	55.3%	9.7%
SnS_2:Ge20%	29.7%	51.5%	18.8%
SnS_2:Ge30%	23.4%	41.8%	34.8%

(b) Sn-S-N compositions from RBS & ERD:

Label	Sn	S	N
SnS_2:N20%	38.4%	42.6%	19.0%
SnS_2:N25%	31.4%	44.2%	24.4%
SnS_2:N30%	28.3%	41.0%	30.7%

(c) Sn-S-Si compositions from RBS:

Label	Sn	S	Si
SnS_2:Si10%	33.7%	52.4%	13.9%
SnS_2:Si20%	27.5%	50.6%	21.9%
SnS_2:Si30%	23.4%	43.5%	33.1%

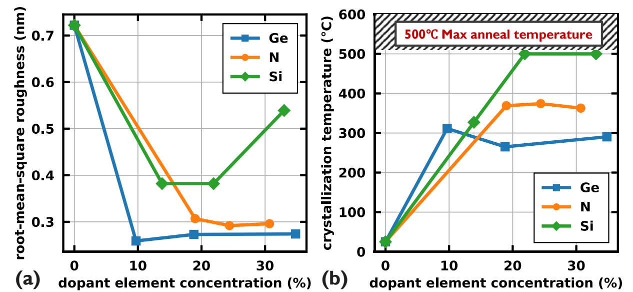

Fig.3. (a) RMS roughness measured by AFM for various dopant concentrations. Amorphous doped materials are smoother than the crystalline reference. (b) Crystallization temperature extracted by in-situ XRD analysis.

free OTS ternary materials for both selector and self-rectifying memory device applications [3,4]. We provide insights into the link between chemical composition, thermal stability, and electrical performance of these materials in device structures integrated on 300mm wafers with an industry-relevant process flow. By doing so, we contribute to the advancement of sustainable semiconductor technologies and pave the way for their integration into future electronic devices.

The remainder of this paper is organized as follows. Section II provides the details about the blanket film properties focusing on thermal stability and defectivity. In Section III, we report the

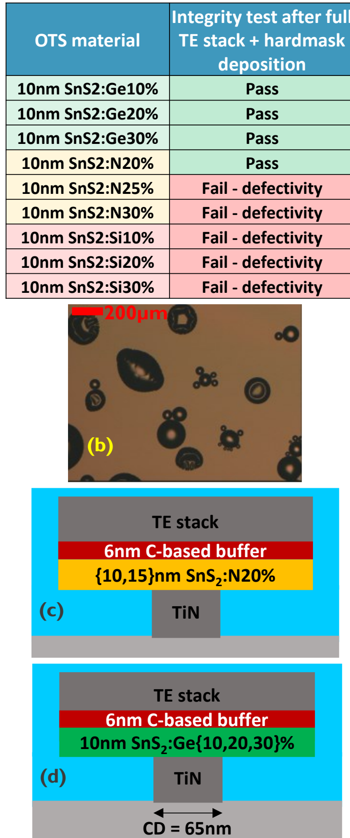

OTS material	Integrity test after full TE stack + hardmask deposition
10nm SnS2:Ge10%	Pass
10nm SnS2:Ge20%	Pass
10nm SnS2:Ge30%	Pass
10nm SnS2:N20%	Pass
10nm SnS2:N25%	Fail - defectivity
10nm SnS2:N30%	Fail - defectivity
10nm SnS2:Si10%	Fail - defectivity
10nm SnS2:Si20%	Fail - defectivity
10nm SnS2:Si30%	Fail - defectivity

Fig.4. (a) Overview of the stack integrity for various compositions. (b) Defectivity observed for the films with Si and high N content after processing the TE and hard mask for etching. Only composition that pass the test are integrated in mushroom-like device structures with thickness/composition combinations shown in (c) and (d).

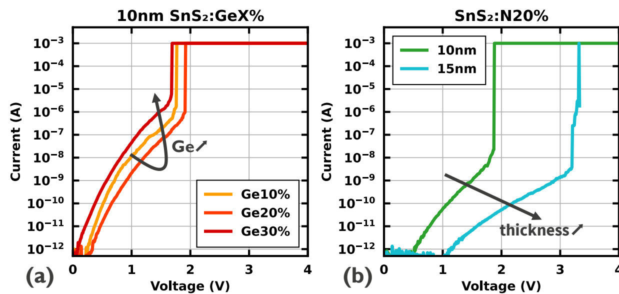

Fig.5. (a) Median initial DC I-V characteristics of integrated OTS devices for (a) Sn-S-Ge and (b) Sn-S-N.

electrical performance results for OTS-selector and OTS-memory applications, including TEM chemical analysis and benchmarking. Finally, Section IV concludes the paper, summarizing the findings and discussing their implications for future research and development in the field.

II. Thin Film Characteristics

Sn-S-Ge and Sn-S-Si films are deposited by co-sputtering from a SnS_2 sputtering target (ST) together with Ge and Si STs, respectively. Ge-Sn-N films are deposited by sputtering from a SnS_2 ST while adding N_2 gas to the sputtering gas. Chemical compositions are tuned by varying the ST sputtering powers or

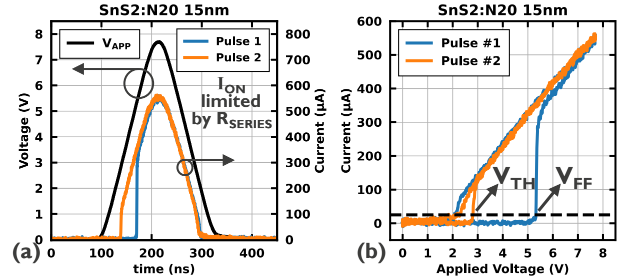

Fig.6. (a) Median AC characteristics of Sn-S-N. (a) current response under triangular pulse (7.5V, 100ns rise/fall time) for two consecutive pulses. (b) Corresponding AC I-V showing the

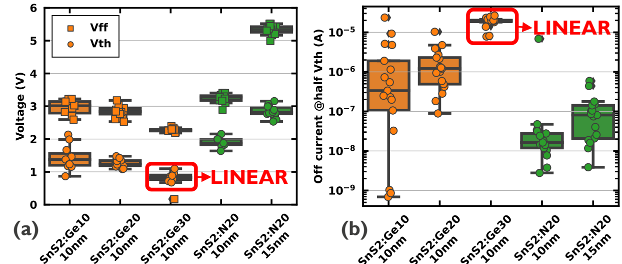

Fig.7. (a) V_{FF} and V_{TH} extracted in AC (triangular pulse, 7.5V peak voltage, 100ns rise/fall time) and (b) I_{OFF} distributions of all tested compositions. I_{OFF} is measured in DC at a voltage equal to half of the threshold voltage extracted from AC measurement. 30% Ge concentration results in a device that does not survive the FF. event, with linear (non-selective) characteristics after the 1st pulse. On-chip R_{SERIES} limits the I_{ON} to ~500µA.

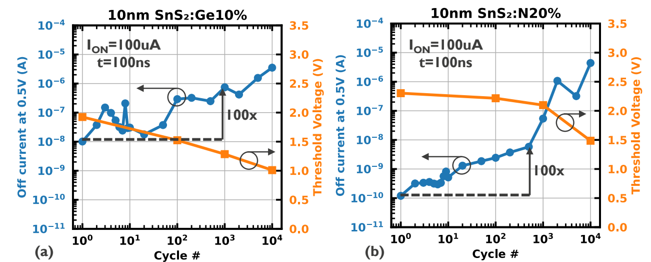

Fig.8. Median endurance characteristics for (a) SnS_2:$Ge_{10\%}$ and (b) SnS_2:$N_{20\%}$. V_{TH} and I_{OFF} rapidly degrade with cycling, with 100X I_{OFF} increase within 1k cycles.

the N_2 gas flow. 15nm-thick blanket films are deposited on SiO_2 substrates.

The actual composition of the films is measured by a combination of Rutherford Backscattering Spectrometry (RBS) and Elastic Recoil Detection (ERD) analyses. The ternary diagrams of Fig. 2 show the compositions identified from ab initio for (a) Sn-S-Ge, (c) Sn-S-N and (e) Sn-S-Si, together with the actual compositions of the deposited films. Composition details are listed in Table I.

The crystalline structure of as-deposited films, capped by a 5nm TiN layer, is evaluated by XRD. From the XRD traces of Fig. 2 it can be observed that the reference SnS_2 film is crystalline, while (b) Ge, (d) N and (f) Si doping in all concentrations results in amorphous as-deposited films. The roughness of uncapped films is evaluated by AFM. Surface roughness data reported in Fig. 3a shows that all the amorphous ternary alloys display smoother surface compared to the

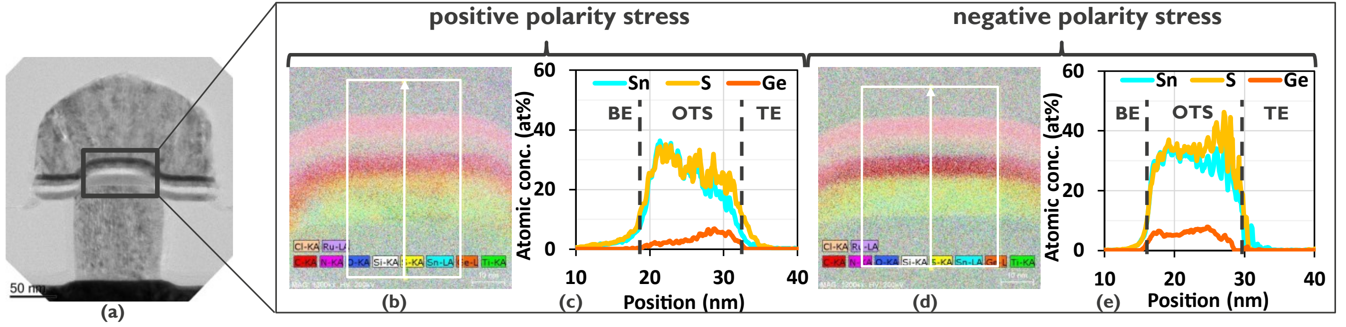

Fig.9. (a) TEM image of SnS2:Ge10% device with CD=100nm. (b) EDX chemical composition map of a device after a positive polarity (10 triangular pulses +3.5V/10μs, Iop~600μA). (c) Vertical line scan shows elemental segregation and non-uniformity. (d, e) Negative polarity stress (10x pulses with −3.5V/10μs) results in a different profile compared to the positive polarity case.

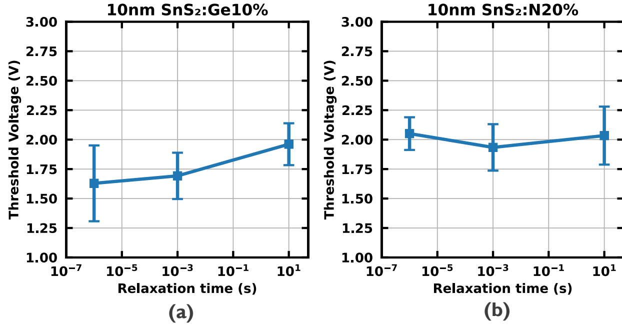

Fig.10. Drift characteristics, i.e. the evolution of the V_{TH} for increasingly longer relaxation times between a first switching pulse and subsequent VTH extraction pulse, of (a) 10nm SnS_2:$Ge_{10\%}$ and (b) 10nm SnS_2:$N_{20\%}$.

crystalline SnS_2 reference.

The crystallization temperature of capped films is extracted by in-situ heated XRD technique and is reported in Fig. 3b. Ge-doped films have the lowest crystallization temperature around 300°C. N doping results in crystallization temperatures approaching 400°C. Si doped films have the highest crystallization temperature exceeding 500°C (value capped by maximum annealing temperature).

Prior to the integration of the newly developed materials in device structures, we evaluate the robustness of the films by testing the stack integrity after the deposition of the full top electrode (TE) and hard mask (HM) for patterning. The result is summarized in Fig. 4. For films with Si and high N contents (≥25%), blisters appear (Fig. 4b), because of thermal/mechanical failure of the stack. For the Si doped films, we also observed an enhanced sensitivity to moisture, causing layer degradation that may also contribute to the failure of the stack. SnS_2:Ge_x and SnS_2:$N_{20\%}$ passed the test and could be tested electrically in device structures with thickness/composition combinations shown in Fig. 4c and 4d.

III. OTS Device Performance

Mushroom-type device structures are fabricated on 300mm wafers. The diameter of the TiN bottom electrode, which defines the size of the active device region, is 65nm for electrical characterization structures and 100nm for TEM characterization structures. The TE material is carbon-based. The reported electrical characteristics are medians of 17 devices

TABLE II
Summary of the Main Material and Device Performance Metrics of the Newly Developed Materials.

	Sn-S-Ge	Sn-S-N	Sn-S-Si
Crystallization temperature	T_X≅300°C	300°C<T_X<400°C	T_X≥500°C
Full hardmask stack robustness	Good	OK only at low N%	Poor
V_{TH} (I_{ON}~500μA)	1.2V (10%Ge)	1.9V (20%N)	No device integration due to defectivity
Selectivity relative to I_{ON}=500μA	8E2 (10%Ge)	1E4 (20%N)	
Endurance	<1E3	<1E3	

uniformly distributed across the wafer unless otherwise mentioned. Fig. 5a shows the initial DC I-V characteristics of 10nm thick Sn-S-Ge OTS for various Ge doping concentrations. Relatively small modulation of the initial characteristics is observed, with smallest initial leakage achieved for 20% Ge concentration. Fig 5b shows the strong impact of the film thickness on the initial characteristics of SnS_2:$N_{20\%}$, with smaller subthreshold current for thicker film.

The time-resolved response to two consecutive pulses is shown in Fig. 6a. The corresponding AC I-V characteristics are plotted in Fig.6b. The first-fire (FF) voltage (V_{FF}) and threshold voltage (V_{TH}) are extracted at a current level of 15μA. Fig. 7a reports the V_{FF} and V_{TH} distributions of all tested compositions. For Sn-S-Ge, 30% Ge concentration results in a device that does not survive the FF event, leading to linear, non-selective, characteristics. Fig 7b shows the distributions of the off current (I_{OFF}) measured in DC at a voltage equal to ½V_{TH}.

The compositions with the smallest I_{OFF} for each material system, i.e. SnS_2:$Ge_{10\%}$ and SnS_2:$N_{20\%}$ are selected for the evaluation of the endurance, drift, and polarity-dependent memory characteristics. The endurance performance for the two compositions is reported in Fig. 8a and 8b, respectively. V_{TH} decreases with cycling, while the I_{OFF} measured at 0.5V progressively increases with cycling, leading to a high leakage state failure. For both studied compositions, I_{OFF} is degraded by a factor of 100 in less than 1E3 cycles. The rapid endurance degradation suggests that the studied materials can undergo structural or compositional changes under the effect of electrical stress or thermal gradients, because of large elemental

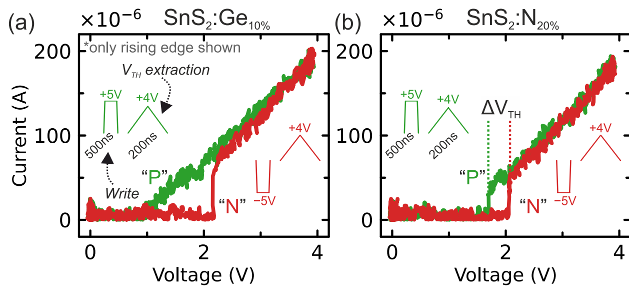

Fig.11. OTS-memory effect in (a) 10nm SnS_2:$Ge_{10\%}$ and (b) 10nm SnS_2:$N_{20\%}$ as a results of opposite polarity programming pulse. Curves labelled as "P" and "N" correspond to the IV characteristics measured after a programming pulse with positive and negative polarity, respectively. In both materials, a clear shift of the AC characteristics is visible. Threshold switching for SnS_2:$Ge_{10\%}$ occurs at lower voltage and is not clearly visible in the graph.

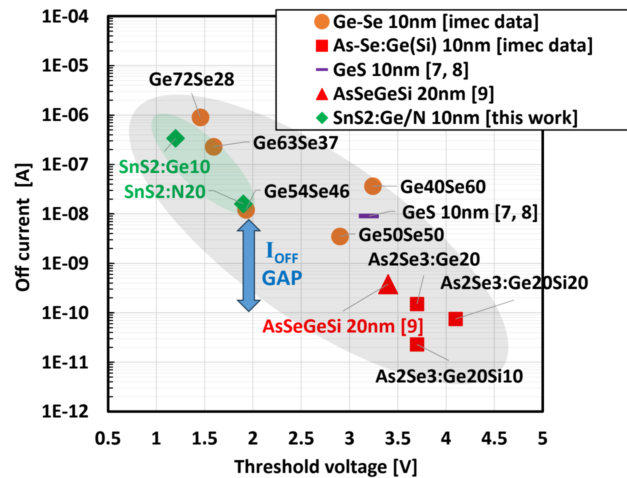

Fig.12. Benchmarking of I_{OFF} and V_{TH} performance metrics of new materials compared to existing As- and Se-based solutions. I_{OFF} is measured at half of V_{TH}.

interdiffusivity.

To confirm this hypothesis, we performed Transmission Electron Microscopy (TEM) inspection and chemical composition analysis for SnS_2:$Ge_{10\%}$ (Fig. 9). We chose to perform TEM and Energy Dispersive X-ray (EDX) analysis on the SnS_2:$Ge_{10\%}$ material because it exhibited the most significant change in V_{TH} during the endurance test. This substantial V_{TH} change provided a higher likelihood of detecting and appreciating atom movements within the accuracy and resolution limitations of our analysis tools. The EDX analysis shown in Figs. 9b-9c provides critical insights into the elemental composition and distribution within the SnS_2:$Ge_{10\%}$ devices after being subjected to electro-thermal stress. The TEM image (Fig. 9a) reveals the overall structural integrity of the device, while the EDX chemical composition maps (Figs. 9b and 9d) highlight the elemental segregation occurring under different stress conditions.

For devices stressed with positive polarity pulses, the EDX map and corresponding vertical line scan (Figs. 9b and 9c) indicate significant elemental segregation and non-uniformity, suggesting that positive polarity stress induces a pronounced redistribution of elements within the device. This is particularly evident from the increased concentration of Ge and the non-uniform distribution of Sn and S. In contrast, negative polarity stress (Figs. 9d and 9e) results in a different profile, demonstrating that the elemental redistribution varies significantly depending on the polarity of the applied stress.

These findings reveal the inherent instability of the SnS_2:$Ge_{10\%}$ material under operational conditions, which is likely due to the high elemental diffusivity. Such segregation can lead to performance degradation, impacting the endurance and reliability of the device. Consequently, strategies to mitigate this, such as doping with additional elements (e.g., Si), may enhance the stability of the material by increasing the crystallization temperature and reducing diffusivity [5, 9]. This is supported by the results of Fig. 3b, showing that Si is the most effective dopant for increasing the crystallization temperature.

Fig. 10 reports the drift characteristics of SnS_2:$Ge_{10\%}$ and SnS_2:$N_{20\%}$ devices, i.e. the measure of the evolution of the V_{TH} for increasingly longer relaxation times between a first switching pulse and subsequent V_{TH} extraction pulse. For the Ge-doped material, a trend of increasing V_{TH} to larger values appears, which can be explained by the natural relaxation of the amorphous material [6]. For the N-doped material, it appears that the V_{TH} is relatively stable in the considered time range between 1ms and 10s. However, it should be noted that, in both cases, the observed trends must be attributed to the convolution of two competing phenomena: i) V_{TH} degradation to lower values due to electrical stress, which for these materials occurs rapidly as observed in the endurance tests of Fig. 8, and ii) actual V_{TH} drift to higher values due to structural relaxation. Given the challenging characterization of the V_{TH} drift in these materials affected by limited endurance, we avoid reporting specific drift coefficient values.

In addition to selector performance metrics, we also evaluate the memory effect resulting from programming pulses with opposite polarities. Figure 11 demonstrates the memory effect observed in SnS_2:$Ge_{10\%}$ and SnS_2:$N_{20\%}$ devices, characterized by a threshold voltage (V_{TH}) window of few hundreds millivolts. This memory window is obtained by applying programming pulses with opposite polarities, indicating the potential use of the doped Sn-S material system for selector-only memory applications [3, 4].

Table II provides a summary of the main material and device performance metrics of the newly developed materials. The benchmarking of the new Sn-S-based materials against existing As- and Se-based solutions, as shown in Fig. 12, highlights the trade-off between off-current (I_{OFF}) and threshold voltage (V_{TH}). The new materials, specifically SnS_2:$Ge_{10\%}$ and SnS_2:$N_{20\%}$, follow the same trend line as established chalcogenides, including As- and Se-free material GeS [7, 8], indicating that they are competitive alternatives.

However, there is a notable performance gap in the I_{OFF}, which is more than 100 times higher than the state-of-the-art materials [9]. This elevated leakage current suggests that further optimization of the material composition is necessary to reduce the I_{OFF}. Targeting compositions with larger trap/mobility gap

values could be a viable approach to achieve this balance, as demonstrated in other chalcogenide material families [10].
The current results validate the ab-initio screening methodology used to identify these materials but also point to the need for additional refinement. Enhancing the screening process to include robustness against atmospheric moisture and expanding to quaternary compositions with lower elemental diffusivity could significantly improve the endurance and overall performance of these materials.

IV. Conclusion

In this paper, we demonstrate the electrical functionality of newly designed Sn-S-based OTS selector and self-selecting memory, validating our ab-initio methodology for the screening of new, sustainable materials. While electrical performance is far from As- and Se-based state-of-art materials, the experimental results allow us to refine our theoretical model. Future work will aim at improving the OTS performance prediction capabilities by a) including selection filters for the robustness against atmospheric moisture, b) adjusting the target mobility gap window to reduce I_{OFF} and c) expanding the screening procedure to quaternary compositions with lower elemental diffusivity for better endurance performance.

Acknowledgment

The authors acknowledge D. Matsubayashi for valuable contributions to the ab-initio screening.

References

[1] D. Matsubayashi et al., "OTS Physics-based Screening for Environment-friendly Selector Materials," 2022 International Electron Devices Meeting (IEDM), San Francisco, CA, USA, 2022, pp. 8.6.1-8.6.4, doi: 10.1109/IEDM45625.2022.10019445.
[2] S. Clima et al, “In silico screening for As/Se-free ovonic threshold switching materials,” npj Comput Mater 9, 96 (2023), doi: 10.1038/s41524-023-01043-2.
[3] S. Hong et al., "Extremely high performance, high density 20nm self-selecting cross-point memory for Compute Express Link," 2022 International Electron Devices Meeting (IEDM), San Francisco, CA, USA, 2022, pp. 18.6.1-18.6.4, doi: 10.1109/IEDM45625.2022.10019415.
[4] T. Ravsher et al., "Self-Rectifying Memory Cell Based on SiGeAsSe Ovonic Threshold Switch," in IEEE Transactions on Electron Devices, vol. 70, no. 5, pp. 2276-2281, May 2023, doi: 10.1109/TED.2023.3252491.
[5] D. Garbin et al., "Composition Optimization and Device Understanding of Si-Ge-As-Te Ovonic Threshold Switch Selector with Excellent Endurance," 2019 IEEE International Electron Devices Meeting (IEDM), San Francisco, CA, USA, 2019, pp. 35.1.1-35.1.4, doi: 10.1109/IEDM19573.2019.8993547.
[6] S. Clima et al. "Ovonic threshold-switching Ge_xSe_y chalcogenide materials: stoichiometry, trap nature, and material relaxation from first principles." physica status solidi (RRL)–Rapid Research Letters 14.5 (2020): 1900672, doi: 10.1002/pssr.201900672.
[7] S. Jia et al. Ultrahigh drive current and large selectivity in GeS selector. Nat Commun 11, 4636 (2020), doi: 10.1038/s41467-020-18382-z.
[8] S. Jia et al. "Scalability of sulfur-based ovonic threshold selectors for 3D stackable memory applications." physica status solidi (RRL)–Rapid Research Letters 15.6 (2021): 2100084, doi: 10.1002/pssr.202100084.
[9] H. Y. Cheng et al., "Si Incorporation into AsSeGe Chalcogenides for High Thermal Stability, High Endurance and Extremely Low Vth Drift 3D Stackable Cross-Point Memory," 2020 IEEE Symposium on VLSI Technology, Honolulu, HI, USA, 2020, pp. 1-2, doi: 10.1109/VLSITechnology18217.2020.9265039.
[10] S. Clima et al., “Ovonic Threshold Switch Chalcogenides: Connecting the First-Principles Electronic Structure to Selector Device Parameters”, ACS Appl. Electron. Mater. 2023, 5, 1, 461–469, doi: 10.1021/acsaelm.2c01458.